Skeletal dosimetry based on μCT images of trabecular bone: Update and comparisons

R Kramer[1], V F Cassola[1], J W Vieira [2, 3], H J Khoury[1], C A B de Oliveira Lira[1] and K Robson Brown[4]

[1] Department of Nuclear Energy, Federal University of Pernambuco, Avenida Prof. Luiz Freire, 1000, CEP 50740-540, Recife, Brazil

[2] Federal Institute of Education, Science and Technology of Pernambuco, Recife, Brazil

[3]Polytechnic School of Pernambuco, University of Pernambuco, Recife, Brazil

[4] Imaging Laboratory, Department of Archaeology and Anthropology, University of Bristol, Bristol, UK

ABSTRACT

Two skeletal dosimetry methods using μCT images of human bone have recently been developed: the Paired-Image Radiation Transport (PIRT) model introduced by researchers at the University of Florida (UF) in the U.S. and the systematic-periodic cluster (SPC) method developed by researchers at the Federal University of Pernambuco in Brazil. Both methods use μCT images of trabecular bone (TB) to model spongiosa regions of human bones containing marrow cavities segmented into soft tissue volumes of active marrow (AM), trabecular inactive marrow (TIM) and the bone endosteum (BE), which is a 50 μm thick layer of marrow on all TB surfaces and on cortical bone (CB) surfaces next to TB as well as inside the medullary cavities. With respect to radiation absorbed dose, the AM and the BE are sensitive soft tissues for the induction of leukaemia and bone cancer, respectively. The two methods differ mainly with respect to the number of bone sites and the size of the μCT images used in Monte Carlo (MC) calculations and they apply different methods to simulate exposure from radiation sources located outside the skeleton. The PIRT method calculates dosimetric quantities in isolated human bones while the SPC method uses human bones embedded in the body of a phantom which contains all relevant organs and soft tissues. Consequently, the SPC method calculates absorbed dose to the AM and to the BE from particles emitted by radionuclides concentrated in organs or from radiation sources located outside the human body in one calculation step. In order to allow for similar calculations of AM and BE absorbed doses using the PIRT method, so-called dose response functions (DRFs) have been developed based on absorbed fractions of energy for electrons isotropically emitted in skeletal tissues. The DRFs can be used to transform the photon fluence in homogeneous spongiosa regions into absorbed dose to AM and BE. This paper will compare AM and BE absorbed fractions of energy (AFs) from electrons emitted in skeletal tissues calculated with the SPC and the PIRT method and AM and BE absorbed doses and AFs calculated with PIRT-based DRFs and with the SPC method. The results calculated with the two skeletal dosimetry methods agree well if one takes the differences between the two models properly into account. Additionally, the SPC method will be updated with larger μCT images of TB.

1. Introduction

Recently, two methods for skeletal dosimetry based on μCT images of human bone have been proposed: First, the Paired-Image Radiation Transport (PIRT) model introduced by researchers at the University of Florida (UF) in the U.S. (Shah et al 2005) and second, the systematic-periodic cluster (SPC) method developed by researchers at the Federal University of Pernambuco in Brazil (Kramer et al 2006, 2007). Both methods use μCT images of trabecular bone (TB) to model spongiosa regions of human bones containing marrow cavities segmented into soft tissue volumes of active marrow (AM), trabecular inactive marrow (TIM) and bone endosteum (BE). In the adult skeleton, AM is distributed throughout the trabecular marrow cavities of the skeleton, except in the lower long bones and lower parts of the upper long bones, while the BE, also called shallow marrow, is represented by a 50 μm thick layer of marrow on all TB surfaces and on cortical bone (CB) surfaces next to TB as well as inside the medullary cavities.

Using the EGSnrc Monte Carlo (MC) code (Kawrakow and Rogers 2003), both methods calculate absorbed fractions and specific absorbed fractions of energy, as well as absorbed or equivalent dose to the AM (tissue at risk for leukaemia induction) and to the BE (tissue at risk for bone cancer induction) from electron emitting radionuclides concentrated in skeletal tissues. Both, the PIRT and the SPC method, transport electrons in spongiosa regions by introducing a microstructure volume based on μCT images of TB, which is often used repeatedly because the spongiosa dimensions of a particular bone may exceed the dimensions of the imaged bone sample.

Apart from several conceptual differences to be discussed in this paper, the two skeletal dosimetry models apply different methods to simulate exposure from radiation sources located outside the skeleton. The PIRT method calculates dosimetric quantities in isolated human bones while the SPC method uses human bones embedded in the body of a phantom which contains all relevant organs and soft tissues. Consequently, the SPC method calculates absorbed dose to the AM and to the BE from particles emitted by radionuclides concentrated in organs or from radiation coming from sources located outside the human body in one calculation step. In order to allow for similar calculations of AM and BE absorbed doses using the PIRT method, so-called "dose response functions" (DRFs) for photon radiation have been developed based on absorbed fractions of energy for electrons isotropically emitted in skeletal tissues (Hough et al 2011, Johnson et al 2011). The DRFs can be used to transform the photon fluence in homogeneous spongiosa regions into absorbed dose to AM and BE.

The influence of parameters such as the micro voxel resolution, the trabecular bone volume fraction (TBVF), the bone site, the donor of the bone sample and the size of the extracted μCT image, called cluster, on the skeletal soft tissue absorbed doses has been investigated in previous publications using the SPC method (Kramer et al 2006, 2007). At the time however, the influence of the cluster size on dosimetric results was studied only for μCT images from one lumbar vertebra and only for external whole body exposure to photons (Kramer et al 2009). Here, the influence of the size of the μCT images on skeletal soft tissue absorbed doses will be studied using five different bone-specific μCT images representative for the adult human skeleton and simulating whole and partial body exposure to photons and electrons from external and internal radiation sources in order to find out if an update of actual SPC MC codes with larger clusters is necessary.

Comparisons between the SPC and the PIRT methods have already been made in the past for a femoral bone sample (Kramer et al 2011), however, after the publication of new data by the UF research group (Hough et al 2011, Johnson et al 2011) a more comprehensive study became possible. In particular, this paper will compare AM and BE absorbed fractions of energy from electrons emitted in skeletal tissues calculated by the SPC and the PIRT method. Additionally, a comparison will be made between AM and BE absorbed doses and AFs calculated with PIRT-based DRFs and with the SPC method.

2. Materials and methods

One purpose of this study is to investigate dosimetric effects as a function of the μCT image size used by the SPC method, but not to change the SPC method as such or to propose a new method. Therefore only a short summary of the SPC method will be presented based on descriptions given earlier (Kramer et al 2006, 2007, 2009, 2010, 2011).

2.1 The standing FASH3 and MASH3 phantoms

Originally developed in 2010 by Cassola et al, FASH3 and MASH3 represent the third edition of the mesh-based adult human phantoms in standing posture (Cassola et al 2011). FASH3 and MASH3 have standing heights, total body masses as well as organ and tissue masses according to ICRP89 (ICRP 2002). Figures 1a and 1b show the surface and the skeleton, respectively, of the FASH3 phantom. Corresponding images for the MASH3 phantom are shown in figures 2a and 2b.

For the purpose of radiation transport calculations, especially for skeletal dosimetry investigations, the phantoms were voxelized with a cubic voxel resolution of 1.2 mm. Then, the skeletons of both phantoms were segmented into regions of cortical bone, spongiosa, medullary cavities and cartilage based on data taken from ICRP publications (ICRP 1995, 2002). TB samples from five different bone sites (frontal bone of the cranium, sternum, lumbar vertebra (L1), iliac crest and femur) were extracted from a 30 year old female skeleton and scanned at the Imaging Laboratory of the Department of Archaeology and Anthropology, University of Bristol, Bristol, UK at 60 μm resolution using a μCT scanner Skyscan 1172 (Skyscan Corporation, 2630 Aartselaar, Belgium) with 80 kV (100 μA). After segmentation of the μCT images into TB and marrow cavities, the TBVFs were found to be 11.4% for the sternum, 11.3% for the vertebra, 21.2% for the pelvis, 51.6% for the cranium and 15.2% for the femur which is in good agreement with corresponding TBVFs given by ICRP70 (ICRP 1995) for adults. The images from the frontal bone, sternum, lumbar vertebra, iliac crest and femur were used for the cranium and mandible, for the rib cage, for the spine/sacrum, for the pelvis and for the long bones, respectively.

2.2 The μCT image size

During MC calculation with the EGSnrc code, particles are transported through the phantom's 1.2mm macro voxel matrix. If a particle enters a spongiosa macro voxel, MC transport is transferred to the 60 μm micro matrix of the corresponding μCT image of TB. To this end the spongiosa macro voxel is replaced by a 1.2mm cube of trabecular microstructure, called micro matrix, containing 20 x 20 x 20 = 8000 micro voxels with a cubic size of 60 μm. A parallelepiped of a number of micro matrices is called a 'cluster'. Using only a limited range of exposure scenarios, a previous study came to the conclusion that a cluster with only 2 x 2 x 2 = 8 micro matrices is sufficient to produce reliable and consistent dosimetric results (Kramer et al 2009). In order to re-check this conclusion the maximum extractable image size for the five bone samples was determined. It was found that a cluster of 8 x 3 x 8 = 192 micro matrices could be extracted from each of the five μCT images which represents a 9.6 mm x 3.6 mm x 9.6 mm parallelepiped of spongiosa volume, being 24 times larger than the cluster with 8 micro matrices. Extraction of the 8 and the 192 micro matrix clusters from the μCT images was based on the criterion of equal TBVF.

2.3 AM, TIM and BE segmentation

Once the EGSnrc code has read the macro voxel matrix of the phantom and the five bone site specific clusters of micro matrices, the code segments AM, TIM and BE in the marrow cavities based on cellularity factors (CFs) and BE thickness defined by the user and finally calculates the corresponding

skeletal tissue volumes and masses. This two-step procedure of skeletal tissue segmentation preserves the original trabecular microstructure as given in the μCT images, while at the same time it is possible to provide a flexible segmentation of AM, TIM and BE at runtime according to actual values for CFs and BE thickness.

Skeletal tissue volumes and masses for the FASH3 and the MASH3 phantoms resulting from the two-step segmentation process are shown in table 1. The cellularity factors used for this segmentation were ribcage = 0.6, spine/sacrum = 0.7, pelvis = 0.48, long bones = 0.25 and cranium/mandible = 0.38 based on ICRP70 (ICRP(1995). 50 μm was used for the BE layer thickness in accordance with ICRP110 (ICRP 2009). Table 1 also shows ICRP reference masses for comparison. Agreement within a margin of 4% with reference values can be observed for cortical bone (CB), active marrow (AM), inactive marrow (IM) and the endosteum (BE), taking into account the revised BE data. TB masses agree within 12 % with reference values. The masses for AM, TIM, TB and BE reflect the original microstructure of the μCT images, i.e. no attempts have been made to adjust them to the ICRP reference values. The cartilage masses for the FASH3 and MASH3 phantoms do not include cartilage located outside the skeleton (ears, nose, etc.) which explains their smaller values compared to the ICRP reference data. Miscellaneous tissues have not been segmented in the phantoms' skeletons. The endosteum is a sub-volume of the marrow (ICRP 2009), i.e. its volume is already included in the volumes of active and inactive marrow and does therefore not contribute to the total skeleton volume or mass shown in table 1.

2.4 The SPC method

Given the segmented skeletal tissue environment described in the previous sections, the SPC method of particle transport through human spongiosa uses clusters of micro matrices in a systematic and periodic manner, i.e. if a particle, when leaving a spongiosa voxel, enters a neighbouring spongiosa voxel it will enter the neighbouring micro matrix in the cluster. If the spongiosa volume of the bone site is larger than the cluster, when leaving the cluster, the particle is re-introduced into the cluster, i.e. the cluster will be used again and again until the particle leaves the spongiosa to enter cortical bone or cartilage. Initially, a random selection of micro matrices was also investigated which made it necessary to clearly define the method finally adopted which is the systematic and periodic use of clusters, called SPC method. Similar to the PIRT method, the SPC method also assumes that the use of the μCT images as discussed above satisfactorily describes the spongiosa region of the corresponding bone.

2.5 Data analysis

The result tables will show pairs of absorbed dose conversion coefficients (CCs) or AFs as a function of the particle energy together with the statistical MC errors and the percentage difference (Pdif) between the CCs or AFs. The Pdif between two CCs or AFs reflects the statistical uncertainties associated with both MC results as well as conceptual differences between the two methods to be compared. In order to identify those Pdifs that can be attributed to differences between the two methods, comparison was made with the error propagation law on 95% confidence:
Let CC_A, CC_B be conversion coefficients and err_A , err_B their absolute statistical MC errors calculated with methods A and B, respectively. If

$$|CC_A - CC_B| > 2 * SQRT\ \{err_A^2 + err_B^2\}$$

then the Pdif = $100*(CC_A - CC_B)/CC_A$ is considered to indicate a "significant percentage difference" (SPD), i.e. the observed difference is interpreted as being caused by conceptual differences between the two methods beyond statistical variations. A corresponding notation will be used for AFs. In the result tables, SPDs are shown in ***red, bold, italic numbers***.

3. Results

3.1 Influence of the Cluster size

Conversion coefficients (CCs) between AM and BE absorbed dose and air kerma as well as AM and BE absorbed fractions of energy (AFs) presented in this section have been calculated with the SPC method using cluster sizes of 2 x 2 x 2 = 8 (8 SPC) and 8 x 3 x 8 = 192 (192 SPC) micro matrices. Associated with each CC or AF is a statistical MC error, determined as coefficient of variance. MC errors are usually smaller than 1%, except for some cases when incident particle energies are smaller than 30 keV. Cluster size results are shown only for the MASH3 phantom, because FASH3 results are very similar. FASH3 results are presented later in section 3.2 on the comparison with PIRT-based data.

External exposure to mono-energetic photons has been simulated for a parallel beam covering the whole body of the phantom for anterior-posterior (AP) direction, rotational incidence around the vertical body axis (ROT) and for an isotropic radioactive cloud in the upper hemisphere (ISO2PI). Incident photon energies varied between 15 keV and 10 MeV, photon cut-off energy was 2 keV in all tissues, electron cut-off energy was 20 keV in tissues located outside the skeleton and 5 keV in all skeletal tissues. Additional calculations were made for the X-ray examinations Abdomen AP and Thorax PA with a divergent beam and collimated field size. Photon cut-off energy was 2 keV in all tissues, electron cut-off energy was 150 keV in tissues located outside the skeleton and 5 keV in all skeletal tissues. Internal exposure has been simulated for mono-energetic photons emitted in the lungs and in the brain as well as for mono-energetic photons and electrons emitted in the AM and the trabecular bone volume (TBV) of the MASH3 phantom. Incident particle energies varied between 15 keV and 4 MeV, cut-off energies were the same as those mentioned before for mono-energetic external exposure.

3.1.1 Photon sources located outside the skeleton

CCs between AM and BE absorbed dose and air kerma free in air (D/AK) for whole body irradiation of the MASH3 phantom have been calculated with 8 and 192 micro matrices for mono-energetic photons between 15 keV and 10 MeV and with equal numbers of source particles. CCs for anterior-posterior (AP) parallel incidence, for rotational parallel incidence perpendicular to the phantom's vertical axis (ROT) and for isotropic incidence from the upper hemi-sphere (radioactive cloud) (ISO2PI) are shown in tables 2a-c, respectively together with their statistical MC errors and the Pdifs.

Tables 2a-c show 102 pairs of CCs, 11 of which have SPDs, 6 for the AM and 5 for the BE, i.e. that about 11% of the Pdifs reflect differences caused by the different cluster sizes, while 89% of the Pdifs are located within the 95% confidence interval (CI) indicating just statistical variations. Only 14 pairs of CCs show Pdifs greater than 2%. At low energies, CCs exhibit small values and consequently already a small absolute difference between two CCs can make a big relative difference as shown by the Pdifs. The data basically confirm similar findings made earlier (Kramer et al 2009), namely that for external whole body exposure to photons AM and BE absorbed doses do not depend significantly on the size of the μCT images of trabecular bone.

CALDose_X, available at www.caldose.org, calculates organ and tissue absorbed doses in the FASH3 and the MASH3 phantoms for conventional X-ray diagnosis (Kramer et al 2008). For the skeletal tissues, CALDose_X uses the cluster with 8 micro matrices and outputs the maximum AM and BE absorbed doses found among the bones located inside the X-ray beam. Comparative calculations have been made here with the two clusters for radiographs of the thorax and of the abdomen applying the commonly used number of five million source photons. The results, expressed as organ and tissue absorbed doses normalized to incident air kerma (D/INAK), are shown in tables 3a-b for the AM, the BE and some other organs and tissues. Compared to the mono-energetic data shown in tables 2a-c, no

SPDs can be found for the AM and the BE Pdifs in tables 3a-b, probably because the spectral distribution of photon energies offsets dosimetric effects seen for mono-energetic radiation earlier in tables 2a-c.

Table 4a presents CCs between AM and BE absorbed doses and cumulated activity (D/Ã) in the ribs from exposure to photons emitted in the lungs, while table 4b shows the same quantities for the cranium from exposure to photons emitted in the brain. Now, radiation sources are located in body organs, but still outside the skeleton. 8 out of 44 ratios show SPDs, 5 for the AM and 3 for the BE, i.e. that 23% of the AM CCs and 14% of the BE CCs reflect cluster size influence in the results. The largest Pdif is 5.97% at 20 keV for the BE in the cranium. Similar to external exposures discussed above, most of the Pdifs are smaller than 2%, many below 1%. Although the appearance of SPDs increased to 18% of the data shown in tables 4a-b, most Pdifs are still within the 95% CI indicating statistical reasons for the Pdifs.

3.1.2 Sources inside the skeleton

This section presents absorbed fractions of energy (AF) for isotropic photon and electron emission in the AM and in the TBV of the MASH3 phantom. AF(AM←AM) and AF(AM←TBV) in the skeleton for photons calculated with the 8 and 192 micro matrix clusters are shown in table 5a. For source tissue AM the larger Pdifs, up to 5.4%, between 10 and 50 keV are all SPDs, which represents more than 40% of the 12 energy points. For energies higher than 50 keV the Pdifs become significantly smaller, well below 1%, and remain within the 95% CI. For source tissue TBV the SPDs dominate the scene: 10 out of 12, or more than 80% of the Pdifs are significant, i.e. that the different trabecular bone structures of the 8 SPC and the 192 SPC clusters are mainly responsible for the differences observed. This fact becomes even more evident in table 5b: For AF(BE←AM) and AF(BE←TBV) all Pdifs are significant. Being a 50 μm layer next to the trabecular bone surface, the BE very sensitively registers different trabecular bones structures in terms of AF or absorbed dose. From 48 pairs of AFs in both tables, 39 show SPDs, i.e. that 81.3% of all data reflect the different trabecular bone structures of the 8 SPC and the 192 SPC clusters. Tables 6a-b show similar AFs for electron emission. 45 from 48 pairs of AFs, or 93.8%, show SPDs. Pdifs within the 95% CI are becoming rare events. With MC errors being very small, it becomes evident that for radiation sources located in skeletal tissues most Pdifs are caused by the different specific trabecular bone structures of the 8 SPC and the 192 SPC clusters in spite of the fact that they have equal TBVFs.

3.2 Comparison with PIRT data

The 192 SPC method for skeletal dosimetry will be compared directly and indirectly with the PIRT method. The direct comparison presented in the next section will look at electron AFs of energy for the AM and the BE calculated with the 192 SPC method in the skeleton of the MASH3 phantom and with the PIRT method in the skeleton of the UFHADM phantom (Hough et al 2011). The indirect comparison to be shown in section 3.2.2 will use so-called “dose response functions” (DRFs) to calculate absorbed dose and AF for the AM and the BE in the skeleton of the FASH3 phantom for exposure to photons. The DRFs have been developed by Johnson et al (2011) based on electron AFs calculated with the PIRT method. The FASH3/DRF results will be compared with the FASH3/192 SPC results.

3.2.1 Comparison with PIRT-based electron AFs

Information on the distribution of tissue volumes in the skeletons of the MASH3 and the UFHADM phantoms is presented in the next two tables. All UFHADM skeletal tissue volumes have been calculated with information provided in table 1 of the paper of Hough et al (2011). Table 7 shows bone site specific volumes for cortical bone, spongiosa and medullary cavity in a theoretical skeleton

based on ICRP70 (ICRP 1995) and ICRP89 (ICRP 2002), in the MASH3 skeleton and in the UFHADM skeleton. The ICRP-based skeletal tissue volumes have been segmented in the bones of the MASH3 skeleton, except for the cervical and thoracic vertebrae, while the UFHADM skeletal tissue volumes have been segmented based on CT images from the cadaver of a 40 year old male (Hough et al 2011). Differences between total cortical bone, spongiosa and medullary cavity volumes of the MASH3 and the UFHADM skeletons are 5%, 6% and 33%, respectively. For specific bones one can see agreement between MASH3 and UFHADM volumes, for cortical bone of the lumbar vertebrae or for the spongiosa of the mandible, for example, but one can also observe differences up to a factor of 10, for the spongiosa of the patellae, for example.

Table 8 presents bone site specific volumes for spongiosa, trabecular bone (TB), active marrow (AM), trabecular inactive marrow (TIM), trabecular bone endosteum (TBE), trabecular bone volume fraction (TBVF) and cellularity factor (CF) for the MASH3 and the UFHADM phantoms. Segmentation of TB, AM, TIM and TBE in the spongiosa of the MASH3 phantom has been described in chapter 2. Except for cellularity factors and the BE thickness, no additional ICRP data have been used to segment AM, TIM and TBE in the μCT images for the MASH3 skeleton. Total TB, AM, TIM and TBE volumes for the MASH3 and the UFHADM skeletons differ by 1%, 3%, 13% and 3%, respectively. Volume differences for specific bones reach from 4% for TB and TBE of the proximal humeri to more than a factor of 5 for the TIM of the scapulae. TBVFs for the two models agree within 2% for the clavicles or 5% for the ribs, but also disagree by more than a factor of 5 for the mandible. Cellularity factors between MASH3 and UFHADM agree, except for the ribs, sternum, clavicles and scapulae because the 192 SPC method uses one CF for the whole rib cage.

In the UFHADM skeletal model, "medullary active marrow" was segmented in the upper halves of the femora and humeri medullary cavities (Hough et al 2011). According to ICRP70 (1995) and ICRP89 (ICRP 2002) the adult medullary cavities do not contain active marrow. Therefore, the skeletal model for the FASH3 and MASH3 phantoms contains only trabecular AM.

In the 192 SPC skeletal model, the trabecular inactive marrow is segmented always in groups of three TIM micro voxels together (Kramer et al 2010), based on a publication by Bolch et al (2002). The paper by Hough et al (2011) does not provide information on how specifically AM and TIM have been segmented in the trabecular marrow cavities. However, the paper explains on page 2327 "Cellularity independent values of Φ (AM $\leftarrow$ r_s) are given next for source regions IM, TBS, TBV, CBS_{HC} and CBV", where Φ (AM $\leftarrow$ r_s) is the specific absorbed fraction in active marrow for arbitrary source regions. From the independence of Φ (AM $\leftarrow$ r_s) from cellularity one can conclude that in the UFHADM skeletal model TIM has been segmented as single micro voxels, but not as groups of micro voxels.

If electrons emitted in skeletal tissues have sufficient energy they can penetrate through the cortical bone layer into soft tissues located outside the skeleton and can even penetrate through cortical bone layers or cartilage of neighbouring bones to contribute to the AFs there. In case of the FASH3 and MASH3 skeletons this cross-fire between neighbouring bones starts at electron energies above 550 keV. The description of the PIRT transport model in the paper of Hough et al (2011) indicates that the calculations of the electron AFs have been made for each bone isolated from the rest of the skeleton, i.e. cross-fire between neighbouring bones was not taken into account by the PIRT model.

In view of the various differences between the exposure models mentioned above one would expect to see many SPDs in the upcoming tables. Absorbed fractions of energy in the AM of the skeletons of the MASH3 and the UFHADM phantoms (Hough et al 2011) from electrons emitted in the AM and in the TBV are shown in table 9a as function of the electron energy between 10 keV and 4 MeV. The statistical MC errors for the UFHADM results are "within 1%" (Hough et al 2011). As expected most Pdifs presented in table 9a are significant, only three low-energy Pdifs for source tissue AM and one Pdif at 10 keV for source tissue TBV can be considered as being just statistical. AF(AM←AM) for the two phantoms agree within 2.5% up to 30 keV and within 10% up to 1 MeV. For higher energies

the Pdifs increases to reach 18.1% at 4 MeV. AF(AM←TBV) Pdifs also increase with increasing electron energy but they are larger: about 10% up to 200 keV, reaching almost 26% at 4 MeV.

Table 9b shows the same quantities but now for the MASH3* phantom, which has TIM segmented like in the UFHADM phantom (= single TIM micro voxels) and the bone cross-fire switched off, i.e. the transport of electrons leaving a bone is immediately terminated. One can see that agreement between the AFs for the two phantoms improved because Pdifs and the number of SPDs became smaller. The different TIM segmentation methods affect the results especially for low energies, while the bone cross-fire effect can be observed at high energies. For example, switching off the bone cross-fire reduces the Pdif between AF(AM←AM) and AF(AM←TBV) for the two phantoms at 4 MeV by 6.3% and by 4%, respectively. Between 10 and 30 keV the AM Pdifs decreased by a factor of 2 due to the use of the PIRT TIM segmentation method. SPDs decreased from 20 in table 9a to 14 in table 9b because the two changes, TIM segmentation and bone cross-fire, reduced differences between SPC and PIRT methods.

Table 10a shows absorbed fractions of energy in the BE of the skeletons of the MASH3 and the UFHADM phantoms from electrons emitted in the AM and the TBV as function of the electron energy between 10 keV and 4 MeV. From 24 pairs of AFs only two have no SPDs, namely at 0.5 and 1.0 MeV for source tissue TBV. On average, Pdifs for the BE AFs are by about a factor of 2 greater than those seen in table 9a for target tissue AM, because differences between the MASH3 and the UFHADM skeletons (TBVF, cavity size, thickness of the trabeculae, etc.) are dosimetrically mostly reflected in the 50 μm layer of the BE next to the trabecular bone surface. Pdifs can reach almost 50% in the case of source tissue TBV at 10 keV.

Table 10b shows the same comparison but now using MASH3*, i.e. TIM was segmented like in the UFHADM phantom (= single TIM micro voxels) and the bone cross-fire was switched off. The change of TIM segmentation has no effect on the AFs(BE←TBV) because per definition the target tissue BE is composed of marrow, either AM or TIM and the source tissue TBV emits electrons independently from the TIM segmentation, while AFs(BE←AM) are affected by the TIM segmentation because the spatial distribution of AM and TIM micro voxels depends on the segmentation method. At 10 keV, the Pdif for the AF(BE←AM) decreases by 5.3% after the change of the TIM segmentation method, for example. Again, switching off the bone cross-fire reduces the difference between MASH3 and UFHADM BE AFs. At 4 MeV, this effect is 5.1% and 2.2% for the source tissues AM and TBV, respectively. Compared to table 10a, AFs(BE←AM) also become smaller after the introduction of the two changes (TIM segmentation and bone cross-fire switch-off), but the number of SPDs does not change: all 12 Pdifs were and remain significant. For source tissue TBV the number of SPDs also remains unchanged, however the Pdifs decrease for energies above 0.5 MeV.

3.2.2 Comparison with dose response functions (DRF)

From the papers of Shah et al (2005) and Hough et al (2011) it is understood that the PIRT code transports electrons in isolated bones of the UFHADM skeleton, i.e. that calculation of AM and BE absorbed dose from external exposure of the UFHADM phantom to photons, for example, cannot be simulated in one calculation step. Therefore, so-called dose response functions (DRFs) for the AM and the BE were developed by Johnson et al (2011) which relate the absorbed dose in the AM or the BE to the photon fluence in the homogeneous spongiosa based on AM and BE AFs calculated by Hough et al (2011) for the UFHADM phantom. The idea of the DRFs is to "decouple the transport of photons and their secondary electrons" (Johnson et al 2011) and thereby enable MC calculations for exposure to photons to be carried out with kerma approximation and at the same time being able to take AM and BE AFs based on μCT images of TB into account.

In order to compare the 192 SPC and the DRF methods, EGSnrc user codes for the MASH3 and the FASH3 phantoms were developed which do not use μCT images of TB but instead tally the photon fluence in homogeneous spongiosa multiplied with bone specific DRFs taken from tables 1-4 of the paper of Johnson et al (2011). The elemental composition of spongiosa was taken from Hough et al (2011).

CCs between AM and BE absorbed dose and air kerma free in air (D/AK) for whole body irradiation of the FASH3 phantom have been calculated with the 192 SPC method and with DRFs for mono-energetic photons between 15 keV and 10 MeV. CCs for anterior-posterior (AP) parallel incidence, for rotational parallel incidence perpendicular to the phantom's vertical axis (ROT) and for isotropic incidence from the upper hemi-sphere (radioactive cloud) (ISO2PI) are shown in tables 11a-c, respectively. From 102 pairs of D/AK CCs, 82 show SPDs, 40 for the AM and 42 for the BE, i.e. that 80.4% of the data reflect the conceptual differences between SPC and DRF methods. AM absorbed doses for the 192 SPC method and the DRFs agree within 4.16% for the irradiation geometries shown in tables 11a-c for energies between 30 keV and 10 MeV. Pdifs for 15 and 20 keV are usually larger but so are the statistical errors associated with the results. BE absorbed doses in tables 11a-c show larger Pdifs especially for small energies, because, as mentioned earlier, dosimetric quantities in the BE are more sensitive to geometrical differences between the specific TB structure of the 192 SPC and the PIRT μCT images than in the AM. Above 150 keV, Pdifs between BE absorbed dose for the192 SPC method and the DRFs are smaller than 5% and therefore similar to those seen before for the AM absorbed doses. For the exposure scenarios shown in tables 11a – c, the EGSnrc code was forced in subroutine AUSGAB to sample electron directions from an isotropic angular distribution instead of using the default distributions for Photo, Compton and Pair Production effects. No SPDs between CCs for default and isotropic emissions were found, at least for the exposure scenarios under consideration here.

AM and BE absorbed fractions (AFs) in the ribs of the FASH3 phantom from exposure to photons emitted in the lungs are shown in table 12, calculated with the 192 SPC method and with DRFs as function of the photon energy. Almost all AFs show SPDs, nevertheless, good agreement between the 192 SPC method and the DRFs can be observed for the AM and BE AFs. Pdifs remain smaller than 4.61% and 11% for the AM and the BE, respectively.

4. Conclusion

4.1 Cluster size

The influence of the μCT image size on AM and BE absorbed dose or AF has been investigated with the SPC method using two different clusters of 8 and 192 micro matrices based on equal TBVF. The analysis of the Pdifs using error propagation with 95% confidence in tables 2 to 6 has shown that the cluster size does influence dosimetric results, especially for exposure to photons or electrons emitted by radionuclides concentrated in skeletal tissues, while for radiation sources located outside the skeleton, especially outside the body, the cluster size effect is less significant or sometimes even negligible. These findings and principal considerations to take utmost advantage of the size of the μCT images of TB led to the decision to update all SPC EGSnrc user codes for the FASH3 and the MASH3 phantoms with the 192 micro matrix clusters. The updated SPC user codes for the EGSnrc MC code are available on www.caldose.org. Photon and electron CCs and AFs posted on the website for download will be replaced by the updated results.

4.2 Comparison with PIRT-based AFs

The MASH3/192 SPC and the UFHADM/PIRT skeletal dosimetry models are different with respect to the number of bone sites, skeletal tissue volumes, TBVFs, CFs, TIM segmentation, bone cross-fire and medullary AM, which explains why one observes large Pdifs between AFs for the two models presented in tables 9a-10b. It was possible to reduce these differences by adopting the TIM segmentation of the UFHADM/PIRT model and by avoiding bone cross-fire which cannot be taken into account by the UF model. In the same way one can imagine to further reduce AF differences between the two models by harmonizing the CFs or by increasing the number of bone sites in the MASH3/192 SPC model. However, apart from being merely a speculation whether these measures would bridge a part of the remaining gap, after that, more adaptations are simply not possible, because the skeletal tissue volumes and TBVFs shown in tables 7 and 8 cannot be changed. They reflect the skeletal tissue volumes and trabecular microstructure of two different individuals. The TBVFs in the μCT images for the pelvis, for example, are 0.212 and 0.100 for the MASH3 and the UFHADM phantom, respectively, representing a difference by more than a factor of 2 which certainly would influence the AFs in the AM and the BE from particles emitted in the TBV. Consequently, one has to accept that differences between AM and BE absorbed doses or AFs calculated with the 192 SPC and the PIRT method will continue to exist in the same way as organ absorbed dose differences between MASH3 and UFHADM would always exist.

4.3 Comparison with DRFs

To our knowledge, the FASH3/MASH3/192 SPC exposure model is currently the only MC code using μCT images of segmented spongiosa which allows for the calculation of AM and BE absorbed doses or AFs in a human phantom from exposure to radiation sources located outside the skeleton in one calculation step. The coding of the SPC method into the EGSnrc MC code was quite challenging and this would certainly also be the case for other MC codes. Therefore, introducing DRFs as proposed by Johnson et al (2011) represents an interesting concept to facilitate the calculation of AM and BE absorbed doses from external exposure to photons. Tables 11a-c show reasonable agreement between the two methods for external whole body exposure to photons. Good agreement can be observed in table 12 for the ribs AM and BE AFs from photon emitters in the lungs. In general, larger Pdifs can be observed for incident photon energies up to 30 keV and more for the BE than for the AM which reflects the different TB structures of the two models. Strictly spoken, the concept of DRFs is based on a distortion of the physical process by using AFs from isotropic electron emission while secondary electrons resulting from photon interactions usually have characteristic angular distributions. However, as mentioned above, forced isotropic secondary electron emission in skeletal tissues for the exposure conditions presented in tables 11a-c could not show conceptual differences when compared to the default angular distributions, i.e. the “distortion” had no visible effect on the results beyond statistical variations. Yet, in view of all the differences between 192 SPC and PIRT mentioned in the previous section, it is rather impressive how well the results of the 192 SPC method and the DRFs agree, at least for the exposure conditions considered here. Based on the results of this study, the DRF concept is a valuable method for skeletal dosimetry for adults when electron transport through μCT images of trabecular bone is not available.

5. Acknowledgement

The authors would like to thank the Conselho Nacional de Desenvolvimento Científico e Tecnológico - CNPq and the Fundação de Amparo à Ciência do Estado de Pernambuco - FACEPE for financial support.

6. References

Bolch W E, Patton P W, Rajon D A, Shah A P, Jokisch D W and Inglis B A 2002 Considerations of Marrow Cellularity in the 3-Dimensional Dosimetric Models of the Trabecular Skeleton *J Nucl Med* **43:**97- 108

Cassola V F, de Melo Lima V J, Kramer R and Khoury H J 2010 FASH and MASH: Female and Male Adult human phantoms based on polygon meSH surfaces. Part I: Development of the anatomy *Phys Med Biol* **55** 133-162

Cassola V F, Milian F M, Kramer R, de Oliveira Lira C A B and Khoury H J, 2011 Standing adult human phantoms based on 10^{th}, 50^{th} and 90^{th} mass and height percentiles of male and female Caucasian populations, *Phys Med Biol* **56** 3749-3772

Hough M, Johnson P, Rajon D, Jokisch D, Lee C and Bolch W 2011 An image-based skeletal dosimetry model for the ICRP reference adult male – internal electron sources *Phys Med Biol* **56** 2309-2346

ICRP 1995 Basic Anatomical and Physiological Data for use in Radiological Protection: The Skeleton. ICRP Publication 70 *(Oxford: Pergamon)*

ICRP 2002 Basic Anatomical and Physiological Data for Use in Radiological Protection: Reference Values ICRP Publication 89 *(Oxford: Pergamon)*

ICRP 2009 Adult Reference Computational Phantoms ICRP Publication 110 *(Oxford: Pergamon)*

Johnson P, Bahadori A A, Eckerman K F, Lee C and Bolch W 2011 Response functions for computing absorbed dose to skeletal tissues from photon irradiation – an update *Phys Med Biol* **56** 2347-2365

Kawrakow I and Rogers D W O 2003 The EGSnrc code system: Monte Carlo simulation of electron and photon transport, *NRC Report PIRS-701*

Kramer R, Khoury H J, Vieira J W and Kawrakow I 2006 Skeletal dosimetry in the MAX06 and the FAX06 phantoms for external exposure to photons based on vertebral 3D-microCT images *Phys Med Biol.* **51** 6265-6289

Kramer R, Khoury H J, Vieira J W and Kawrakow I 2007 Skeletal dosimetry for external exposure to photons based on μCT images of spongiosa from different bone sites *Phys Med Biol. **52** 6697-6716*

Kramer R, Khoury H J and Vieira J W 2008 CALDose_X a software tool for the assessment of organ and tissue doses, effective dose and cancer risk in diagnostic radiology *Phys Med Biol* **53** 6437-6459

Kramer R, Khoury H J, Vieira J W and Robson Brown K A 2009 Skeletal dosimetry for external exposures to photons based on μCT images of spongiosa: Consideration of voxel resolution, cluster size and medullary bone surfaces *Med Phys* **36** 11 5007-5016

Kramer R, Cassola V F, Khoury H J, Vieira J W, de Melo Lima V J and Robson Brown K 2010 FASH and MASH: female and male adult human phantoms based on polygon mesh surfaces: II. Dosimetric calculations, *Phys Med Biol* **55** 163-189

Shah A P, Bolch W E, Rajon D A, Patton P W and Jokisch D W 2005 A Paired-Image Radiation Transport Model for Skeletal Dosimetry *J Nucl Med* **46**, No.2, 344-353

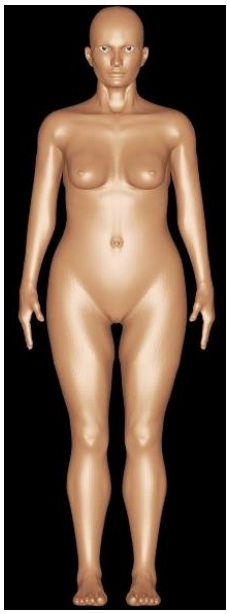

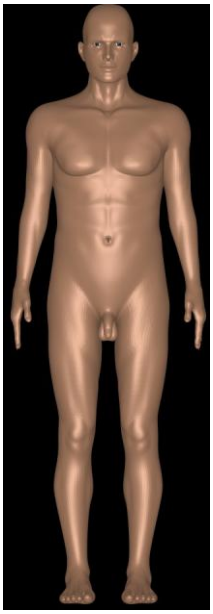
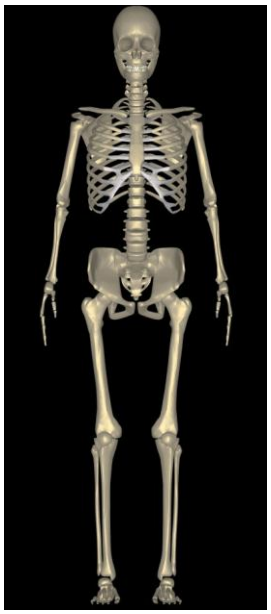

Fig.1a FASH3surface **Fig.1b** FASH3 skeleton **Fig.2a** MASH3 surface **Fig.2b** MASH3 skeleton

Tab 1. Skeletal tissue volumes and masses for the FASH3 and the MASH3 phantoms based on clusters with 192 micro matrices. ICRP masses are shown for comparison.

	FEMALE ADULT					MALE ADULT				
	ICRP110	ICRP89		FASH3		ICRP110	ICRP89		MASH3	
	Mass	Mass	Volume	Density	Mass	Mass	Mass	Volume	Density	Mass
Skeletal tissue	(g)	(g)	(cm^3)	(g/cm^3)	(g)	(g)	(g)	(cm^3)	(g/cm^3)	(g)
Bone, cortical		3200	1643.2	1.92	3154.9		4400	2232.0	1.92	4285.4
Bone, trabecular		800	467.5	1.92	897.5		1100	630.4	1.92	1210.4
Active marrow		900	867.9	1.03	894.0		1170	1176.4	1.03	1211.7
Endosteum, trabecular			319.4	1.00	319.4			431.4	1.00	431.4
Endosteum, medullary			5.4	1.00	5.4			7.0	1.00	7.0
Endosteum, total	407.5*		324.8		324.8	544.4*		438.4		438.4
Inactive marrow, trabecular			1369.8	0.98	1342.4			1881.7	0.98	1843.1
Inactive marrow, medullary			426.5	0.98	418.0			611.1	0.98	598.9
Inactive marrow, total		1800	1796.3		1760.4		2480	2492.6		2442.7
Cartilage		900	582.1	1.10	640.3		1100	686.6	1.10	755.3
Teeth		40	15.4	2.75	42.4		50	15.9	2.75	43.7
Miscellaneous		160					200			
Total skeleton		7800	5372.4	1.38	7389.5		10500	7234.1	1.38	9948.5

*According to Hough et al (2011), the ICRP BE reference masses will be revised to 333 g and 452 g for the female and the male adult, respectively.

Tab 2a. AM and BE absorbed dose per air kerma (D/AK) calculated with 8 and 192 micro matrices for a whole body parallel field of photons incident on the front (AP) of the MASH3 phantom.

External whole body AP

MASH3	Active marrow (AM) Skeleton					Bone endosteum (BE) Skeleton				
Photon	8 SPC		192 SPC		8/192	8 SPC		192 SPC		8/192
Energy	D/AK	Error	D/AK	Error	Pdif	D/AK	Error	D/AK	Error	Pdif
(MeV)	Gy/Gy	%	Gy/Gy	%	%	Gy/Gy	%	Gy/Gy	%	%
0.015	2.559E-04	6.99	2.440E-04	7.16	4.62	2.235E-04	11.93	1.947E-04	13.13	12.88
0.02	0.0044	0.93	0.0042	0.94	***4.55***	5.509E-03	1.30	5.502E-03	1.33	0.12
0.03	0.0584	0.45	0.0572	0.46	***2.05***	0.0985	0.54	0.0960	0.56	***2.54***
0.04	0.2034	0.42	0.2008	0.43	***1.28***	0.3485	0.50	0.3453	0.51	0.92
0.05	0.3933	0.40	0.3955	0.40	-0.56	0.6818	0.48	0.6711	0.49	***1.57***
0.06	0.5646	0.35	0.5695	0.35	-0.87	0.9652	0.43	0.9422	0.44	***2.38***
0.07	0.6943	0.32	0.6977	0.32	-0.49	1.1393	0.40	1.1346	0.41	0.41
0.08	0.7561	0.29	0.7551	0.29	0.13	1.1959	0.38	1.1854	0.39	0.88
0.1	0.8042	0.26	0.8053	0.25	-0.14	1.1918	0.34	1.1858	0.35	0.50
0.15	0.7954	0.31	0.7964	0.31	-0.13	1.0508	0.43	1.0441	0.44	0.64
0.2	0.7777	0.30	0.7794	0.30	-0.22	0.9811	0.41	0.9727	0.42	0.86
0.3	0.7645	0.29	0.7678	0.29	-0.43	0.9223	0.38	0.9134	0.39	0.96
0.5	0.7724	0.29	0.7727	0.29	-0.04	0.9024	0.33	0.8971	0.33	0.59
1	0.8049	0.43	0.8031	0.43	0.22	0.9082	0.40	0.9011	0.40	0.78
3	0.8847	0.48	0.8935	0.48	-0.99	0.9637	0.39	0.9626	0.39	0.11
6	0.9152	0.50	0.9246	0.50	-1.03	0.9848	0.39	0.9821	0.39	0.27
10	0.9193	0.49	0.9062	0.49	***1.42***	0.9590	0.39	0.9505	0.38	0.89

Tab 2b. AM and BE absorbed dose per air kerma (D/AK) calculated with 8 and 192 micro matrices for a whole body parallel field of photons rotational around the vertical body axis (ROT) of the MASH3 phantom.

External whole body ROT

MASH3	Active marrow (AM) Skeleton					Bone endosteum (BE) Skeleton				
Photon	8 SPC		192 SPC		8/192	8 SPC		192 SPC		8/192
Energy	D/AK	Error	D/AK	Error	Pdif	D/AK	Error	D/AK	Error	Pdif
(MeV)	Gy/Gy	%	Gy/Gy	%	%	Gy/Gy	%	Gy/Gy	%	%
0.015	1.613E-04	8.19	1.504E-04	8.44	6.71	3.086E-04	9.42	2.802E-04	10.05	9.20
0.02	0.0036	0.95	0.0035	0.96	***2.78***	0.0057	1.18	0.0056	1.21	1.75
0.03	0.0581	0.42	0.0569	0.43	***2.07***	0.0909	0.52	0.0897	0.53	1.32
0.04	0.2002	0.40	0.1994	0.40	0.40	0.3161	0.49	0.3148	0.50	0.41
0.05	0.3871	0.38	0.3877	0.38	-0.15	0.6094	0.47	0.6108	0.48	-0.23
0.06	0.5445	0.33	0.5440	0.33	0.09	0.8531	0.42	0.8520	0.43	0.13
0.07	0.6626	0.30	0.6639	0.30	-0.20	1.0166	0.39	1.0115	0.40	0.50
0.08	0.7197	0.28	0.7196	0.28	0.01	1.0584	0.37	1.0661	0.38	-0.73
0.1	0.7636	0.24	0.7642	0.24	-0.08	1.0582	0.34	1.0544	0.35	0.36
0.15	0.7545	0.30	0.7576	0.30	-0.41	0.9337	0.43	0.9399	0.44	-0.66
0.2	0.7396	0.29	0.7407	0.29	-0.15	0.8755	0.41	0.8784	0.42	-0.33
0.3	0.7272	0.29	0.7284	0.29	-0.17	0.8209	0.37	0.8294	0.38	-1.04
0.5	0.7319	0.28	0.7326	0.28	-0.10	0.8129	0.32	0.8131	0.33	-0.02
1	0.7635	0.42	0.7651	0.42	-0.21	0.8302	0.39	0.8241	0.39	0.73
3	0.8539	0.46	0.8537	0.46	0.02	0.8989	0.37	0.9033	0.37	-0.49
6	0.8809	0.48	0.8813	0.48	-0.05	0.9146	0.38	0.9205	0.37	-0.65
10	0.8824	0.47	0.8726	0.47	1.11	0.8962	0.37	0.8927	0.36	0.39

Tab 2c. AM and BE absorbed dose per air kerma (D/AK) calculated with 8 and 192 micro matrices for an isotropic field of photons incident from the upper hemisphere (ISO2PI) on the MASH3 phantom.

External whole body ISO2PI										
MASH3	Active marrow (AM) Skeleton					Bone endosteum (BE) Skeleton				
Photon	8 SPC		192 SPC		8/192	8 SPC		192 SPC		8/192
Energy	D/AK	Error	D/AK	Error	Pdif	D/AK	Error	D/AK	Error	Pdif
(MeV)	Gy/Gy	%	Gy/Gy	%	%	Gy/Gy	%	Gy/Gy	%	%
0.015	2.286E-04	7.59	1.982E-04	8.15	13.30	3.956E-04	9.23	3.640E-04	9.70	7.99
0.02	0.0035	1.07	0.0034	1.08	2.86	0.0051	1.38	0.0053	1.39	-3.92
0.03	0.0519	0.49	0.0514	0.50	0.96	0.0806	0.61	0.0814	0.62	-0.99
0.04	0.1759	0.47	0.1744	0.47	0.85	0.2843	0.57	0.2835	0.58	0.28
0.05	0.3356	0.45	0.3366	0.45	-0.30	0.5480	0.55	0.5493	0.56	-0.24
0.06	0.4758	0.39	0.4784	0.39	-0.55	0.7762	0.49	0.7756	0.51	0.08
0.07	0.5847	0.36	0.5836	0.36	0.19	0.9274	0.46	0.9354	0.47	-0.86
0.08	0.6334	0.33	0.6293	0.33	0.65	0.9697	0.43	0.9777	0.44	-0.82
0.1	0.6773	0.29	0.6777	0.29	-0.06	0.9764	0.39	0.9841	0.40	-0.79
0.15	0.6723	0.36	0.6709	0.36	0.21	0.8680	0.49	0.8726	0.50	-0.53
0.2	0.6595	0.34	0.6582	0.34	0.20	0.8182	0.47	0.8148	0.48	0.42
0.3	0.6475	0.33	0.6497	0.33	-0.34	0.7782	0.43	0.7894	0.43	***-1.44***
0.5	0.6684	0.33	0.6645	0.33	0.58	0.7867	0.36	0.7846	0.37	0.27
1	0.7115	0.47	0.7219	0.47	***-1.46***	0.8316	0.43	0.8286	0.43	0.36
3	0.8296	0.51	0.8411	0.51	-1.39	0.9403	0.41	0.9512	0.40	***-1.16***
6	0.8866	0.52	0.8797	0.52	0.78	0.9796	0.41	0.9843	0.40	-0.48
10	0.8812	0.52	0.8837	0.52	-0.28	0.9665	0.40	0.9666	0.39	-0.01

Tab 3a. Organ and tissue absorbed dose per incident air kerma (D/INAK) calculated with 8 and 192 micro matrices for an abdominal radiograph of the MASH3 phantom.

MASH3	Absorbed dose per incident air kerma				
Abdomen, AP, 80 kV, 2.5 mm Al	8 SPC		192 SPC		8/192
Field at detector: 35cm x 40cm	D/INAK	error	D/INAK	error	Pdif
ORGAN/TISSUE	Gy/Gy	%	Gy/Gy	%	%
COLON WALL	0.394	0.32	0.395	0.32	-0.25
KIDNEYS	0.129	0.65	0.128	0.65	0.78
LIVER	0.457	0.14	0.458	0.14	-0.22
LUNGS	0.050	0.51	0.050	0.51	0.00
PANCREAS	0.357	0.57	0.356	0.58	0.28
SMALL INTESTINE WALL	0.331	0.27	0.331	0.27	0.00
SPLEEN	0.293	0.61	0.293	0.61	0.00
STOMACH WALL	0.527	0.44	0.526	0.44	0.19
HEART WALL	0.066	0.87	0.066	0.87	0.00
LYMPHATIC NODES	0.190	0.47	0.189	0.47	0.53
MAXIMUM AM ABSORBED DOSE	0.067	1.10	0.067	1.10	0.00
MAXIMUM BE ABSORBED DOSE	0.086	1.51	0.087	1.59	-1.16

Tab 3b. Organ and tissue absorbed dose per incident air kerma (D/INAK) calculated with 8 and 192 micro matrices for a thoracic radiograph of the MASH3 phantom.

MASH3	Absorbed dose per incident air kerma				
Thorax, PA, 130 kV, 2.5 mm Al	8 SPC		192 SPC		8/192
Field at detector: 35cm x 40cm	D/INAK	error	D/INAK	error	Pdif
ORGAN/TISSUE	Gy/Gy	%	Gy/Gy	%	%
KIDNEYS	0.310	0.53	0.310	0.53	0.00
LIVER	0.157	0.34	0.157	0.34	0.00
LUNGS	0.445	0.22	0.444	0.22	0.22
SPLEEN	0.270	0.82	0.267	0.83	1.11
STOMACH WALL	0.122	1.18	0.122	1.18	0.00
HEART WALL	0.289	0.53	0.288	0.53	0.35
LYMPHATIC NODES	0.129	0.73	0.129	0.73	0.00
MAXIMUM AM ABSORBED DOSE	0.525	0.42	0.526	0.42	-0.19
MAXIMUM BE ABSORBED DOSE	0.729	1.00	0.731	0.93	-0.27

Tab 4a. AM and BE absorbed dose per cumulated activity (D/Ã) in the ribs from photons emitted in the lungs of the MASH3 phantom calculated with 8 and 192 micro matrices.

MASH3	AM(RIBS)←LUNGS					BE(RIBS)←LUNGS				
Photon	8 SPC		192 SPC		8/192	8 SPC		192 SPC		8/192
Energy	D/Ã	Error	D/Ã	Error	Pdif	D/Ã	Error	D/Ã	Error	Pdif
(MeV)	mGy/MBq s	%	mGy/MBq s	%	%	mGy/MBq s	%	mGy/MBq s	%	%
0.015	1.023E-08	1.75	1.001E-08	1.76	2.15	9.068E-09	3.55	9.308E-09	3.42	-2.65
0.02	6.147E-08	0.81	6.249E-08	0.81	-1.66	6.078E-08	1.54	6.154E-08	1.50	-1.25
0.03	1.800E-07	0.55	1.801E-07	0.55	-0.06	2.033E-07	0.97	2.020E-07	0.95	0.64
0.05	2.510E-07	0.57	2.519E-07	0.57	-0.36	3.400E-07	0.93	3.395E-07	0.91	0.15
0.1	3.768E-07	0.44	3.770E-07	0.44	-0.05	4.815E-07	0.79	4.824E-07	0.78	-0.19
0.2	7.087E-07	0.42	7.130E-07	0.42	-0.61	7.757E-07	0.73	7.720E-07	0.72	0.48
0.5	1.682E-06	0.44	1.689E-06	0.44	-0.42	1.739E-06	0.62	1.737E-06	0.61	0.12
1	3.044E-06	0.55	3.066E-06	0.55	-0.72	3.111E-06	0.63	3.091E-06	0.63	0.64
1.5	4.134E-06	0.57	4.204E-06	0.57	***-1.69***	4.219E-06	0.61	4.275E-06	0.61	-1.33
2	5.156E-06	0.58	5.149E-06	0.58	0.14	5.222E-06	0.60	5.206E-06	0.60	0.31
4	8.260E-06	0.56	8.107E-06	0.57	***1.85***	8.369E-06	0.57	8.228E-06	0.57	***1.68***

Tab 4b. AM and BE absorbed dose per cumulated activity (D/Ã) in the cranium from photons emitted in the brain of the MASH3 phantom calculated with 8 and 192 micro matrices.

MASH3	AM(CRANIUM)←BRAIN					BE(CRANIUM)←BRAIN				
Photon	8 SPC		192 SPC		8/192	8 SPC		192 SPC		8/192
Energy	D/Ã	Error	D/Ã	Error	Pdif	D/Ã	Error	D/Ã	Error	Pdif
(MeV)	mGy/MBq s	%	mGy/MBq s	%	%	mGy/MBq s	%	mGy/MBq s	%	%
0.015	3.925E-09	5.22	4.072E-09	4.86	-3.75	3.467E-09	5.79	3.313E-09	5.68	4.44
0.02	2.980E-08	2.06	3.101E-08	2.00	-4.06	2.698E-08	2.32	2.859E-08	2.18	-5.97
0.03	1.749E-07	0.97	1.763E-07	0.96	-0.80	1.850E-07	1.02	1.886E-07	0.97	-1.95
0.05	4.270E-07	0.75	4.405E-07	0.74	***-3.16***	5.448E-07	0.74	5.487E-07	0.71	-0.72
0.1	8.026E-07	0.54	8.315E-07	0.53	***-3.60***	9.824E-07	0.58	1.003E-06	0.55	***-2.10***
0.2	1.573E-06	0.47	1.589E-06	0.47	-1.02	1.702E-06	0.51	1.706E-06	0.49	-0.24
0.5	3.883E-06	0.41	3.924E-06	0.40	-1.06	3.989E-06	0.43	4.044E-06	0.41	***-1.38***
1	7.246E-06	0.42	7.370E-06	0.42	***-1.71***	7.396E-06	0.42	7.457E-06	0.41	-0.82
1.5	1.009E-05	0.41	1.018E-05	0.41	-0.89	1.025E-05	0.41	1.036E-05	0.40	-1.07
2	1.258E-05	0.41	1.261E-05	0.41	-0.24	1.277E-05	0.40	1.283E-05	0.40	-0.47
4	2.115E-05	0.40	2.116E-05	0.40	-0.05	2.145E-05	0.39	2.149E-05	0.39	-0.19

Tab 5a. AM absorbed fractions (AFs) in the whole skeleton from **photons** emitted in the AM and TBV of the MASH3 phantom calculated with 8 and 192 micro matrices.

MASH3										
Photon	Source tissue: Active Marrow, skeleton					Source tissue: Trabecular Bone Volume, skeleton				
Energy	8 SPC	error	192 SPC	error	Pdif	8 SPC	error	192 SPC	error	Pdif
(MeV)	AF(AM←AM)	%	AF(AM←AM)	%	%	AF(AM←TBV)	%	AF(AM←TBV)	%	%
0.01	3.031E-01	0.07	2.913E-01	0.07	***3.89***	6.692E-02	0.17	6.939E-02	0.16	***-3.69***
0.015	1.982E-01	0.09	1.875E-01	0.09	***5.40***	6.477E-02	0.17	6.758E-02	0.16	***-4.34***
0.02	1.433E-01	0.11	1.367E-01	0.11	***4.61***	5.462E-02	0.18	5.692E-02	0.18	***-4.21***
0.03	8.478E-02	0.14	8.313E-02	0.14	***1.95***	3.686E-02	0.21	3.825E-02	0.21	***-3.77***
0.05	4.701E-02	0.18	4.663E-02	0.18	***0.81***	2.248E-02	0.26	2.290E-02	0.26	***-1.87***
0.1	3.559E-02	0.14	3.557E-02	0.14	0.06	1.792E-02	0.20	1.802E-02	0.20	-0.56
0.2	3.687E-02	0.13	3.686E-02	0.13	0.03	1.847E-02	0.18	1.865E-02	0.18	***-0.97***
0.5	3.736E-02	0.14	3.737E-02	0.13	-0.03	1.891E-02	0.18	1.913E-02	0.18	***-1.16***
1	3.402E-02	0.17	3.395E-02	0.17	0.21	1.736E-02	0.22	1.757E-02	0.22	***-1.21***
1.5	3.031E-02	0.18	3.030E-02	0.18	0.03	1.549E-02	0.24	1.568E-02	0.24	***-1.23***
2	2.735E-02	0.19	2.722E-02	0.19	0.48	1.406E-02	0.25	1.424E-02	0.25	***-1.28***
4	1.976E-02	0.23	1.977E-02	0.22	-0.05	1.027E-02	0.29	1.028E-02	0.29	-0.10

Tab 5b. BE absorbed fractions (AFs) in the whole skeleton from **photons** emitted in the AM and TBV of the MASH3 phantom calculated with 8 and 192 micro matrices.

MASH3 Photon	Source tissue: Active Marrow, skeleton					Source tissue: Trabecular Bone Volume, skeleton				
Energy	8 SPC	error	192 SPC	error	Pdif	8 SPC	error	192 SPC	error	Pdif
(MeV)	AF(BE←AM)	%	AF(BE←AM)	%	%	AF(BE←TBV)	%	AF(BE←TBV)	%	%
0.01	4.136E-02	0.21	4.279E-02	0.21	***-3.46***	2.701E-02	0.26	2.584E-02	0.27	***4.33***
0.015	2.921E-02	0.25	3.075E-02	0.24	***-5.27***	2.516E-02	0.27	2.401E-02	0.27	***4.57***
0.02	2.316E-02	0.27	2.448E-02	0.27	***-5.70***	2.234E-02	0.28	2.126E-02	0.28	***4.83***
0.03	1.640E-02	0.31	1.745E-02	0.30	***-6.40***	1.730E-02	0.30	1.644E-02	0.30	***4.97***
0.05	1.165E-02	0.35	1.216E-02	0.34	***-4.38***	1.249E-02	0.34	1.184E-02	0.35	***5.20***
0.1	8.302E-03	0.30	8.626E-03	0.29	***-3.90***	8.886E-03	0.29	8.421E-03	0.30	***5.23***
0.2	7.384E-03	0.27	7.708E-03	0.26	***-4.39***	8.023E-03	0.26	7.587E-03	0.26	***5.43***
0.5	7.244E-03	0.21	7.505E-03	0.21	***-3.60***	7.946E-03	0.20	7.499E-03	0.21	***5.63***
1	6.564E-03	0.21	6.788E-03	0.20	***-3.41***	7.211E-03	0.21	6.783E-03	0.21	***5.94***
1.5	5.843E-03	0.20	6.061E-03	0.20	***-3.73***	6.396E-03	0.20	6.037E-03	0.21	***5.61***
2	5.287E-03	0.21	5.458E-03	0.20	***-3.23***	5.754E-03	0.21	5.423E-03	0.21	***5.75***
4	3.851E-03	0.23	3.988E-03	0.22	***-3.56***	4.104E-03	0.23	3.862E-03	0.23	***5.90***

Tab 6a. AM absorbed fractions (AFs) in the whole skeleton from **electrons** emitted in the AM and TBV of the MASH3 phantom calculated with 8 and 192 micro matrices.

MASH3 Electron	Source tissue: Active Marrow, skeleton					Source tissue: Trabecular Bone Volume, skeleton				
Energy	8 SPC	error	192 SPC	error	Pdif	8 SPC	error	192 SPC	error	Pdif
(MeV)	AF(AM←AM)	%	AF(AM←AM)	%	%	AF(AM←TBV)	%	AF(AM←TBV)	%	%
0.01	9.897E-01	0.01	9.896E-01	0.01	0.01	1.310E-03	1.11	1.321E-03	1.10	-0.84
0.015	9.777E-01	0.01	9.774E-01	0.01	***0.03***	2.757E-03	0.74	2.888E-03	0.73	***-4.75***
0.02	9.629E-01	0.01	9.625E-01	0.01	***0.04***	4.665E-03	0.57	4.725E-03	0.56	-1.29
0.03	9.258E-01	0.01	9.248E-01	0.01	***0.11***	9.261E-03	0.40	9.527E-03	0.39	***-2.87***
0.05	8.333E-01	0.02	8.319E-01	0.02	***0.17***	2.160E-02	0.28	2.225E-02	0.28	***-3.01***
0.1	6.453E-01	0.03	6.424E-01	0.03	***0.45***	5.811E-02	0.16	6.031E-02	0.15	***-3.79***
0.2	5.469E-01	0.03	5.440E-01	0.03	***0.53***	1.314E-01	0.08	1.348E-01	0.08	***-2.59***
0.5	4.672E-01	0.02	4.658E-01	0.02	***0.30***	2.058E-01	0.05	2.065E-01	0.05	***-0.34***
1	4.251E-01	0.03	4.227E-01	0.03	***0.56***	2.012E-01	0.06	2.055E-01	0.06	***-2.14***
1.5	3.922E-01	0.03	3.900E-01	0.03	***0.56***	1.892E-01	0.06	1.934E-01	0.06	***-2.22***
2	3.638E-01	0.03	3.616E-01	0.03	***0.60***	1.769E-01	0.06	1.809E-01	0.06	***-2.26***
4	2.833E-01	0.04	2.820E-01	0.04	***0.46***	1.381E-01	0.07	1.412E-01	0.07	***-2.24***

Tab 6b. BE absorbed fractions (AFs) in the whole skeleton from **electrons** emitted in the AM and TBV of the MASH3 phantom calculated with 8 and 192 micro matrices.

MASH3 Electron Energy (MeV)	Source tissue: Active Marrow, skeleton					Source tissue: Trabecular Bone Volume, skeleton				
	8 SPC AF(BE←AM)	error %	192 SPC AF(BE←AM)	error %	Pdif %	8 SPC AF(BE←TBV)	error %	192 SPC AF(BE←TBV)	error %	Pdif %
0.01	1.403E-01	0.11	1.441E-01	0.11	***-2.71***	2.987E-03	0.73	2.814E-03	0.75	***5.79***
0.015	1.390E-01	0.11	1.424E-01	0.11	***-2.45***	6.300E-03	0.49	5.994E-03	0.50	***4.86***
0.02	1.377E-01	0.11	1.408E-01	0.11	***-2.25***	1.050E-02	0.38	9.900E-03	0.39	***5.71***
0.03	1.332E-01	0.11	1.367E-01	0.11	***-2.63***	2.094E-02	0.26	1.980E-02	0.27	***5.44***
0.05	1.225E-01	0.12	1.256E-01	0.12	***-2.53***	4.654E-02	0.19	4.439E-02	0.20	***4.62***
0.1	1.006E-01	0.11	1.029E-01	0.11	***-2.29***	9.665E-02	0.11	9.376E-02	0.11	***2.99***
0.2	9.168E-02	0.08	9.340E-02	0.08	***-1.88***	1.099E-01	0.07	1.096E-01	0.07	***0.27***
0.5	8.643E-02	0.05	8.972E-02	0.05	***-3.81***	1.053E-01	0.04	1.025E-01	0.04	***2.66***
1	7.969E-02	0.04	8.316E-02	0.04	***-4.35***	9.844E-02	0.04	9.357E-02	0.04	***4.95***
1.5	7.367E-02	0.04	7.691E-02	0.04	***-4.40***	9.197E-02	0.03	8.662E-02	0.03	***5.82***
2	6.812E-02	0.04	7.112E-02	0.04	***-4.40***	8.546E-02	0.03	8.050E-02	0.03	***5.80***
4	5.215E-02	0.04	5.448E-02	0.04	***-4.47***	6.599E-02	0.04	6.156E-02	0.04	***6.71***

Tab 7. Bone site specific volumes for cortical bone, spongiosa and medullary cavity in a theoretical skeleton based on ICRP89 and ICRP70, in the skeleton of the MASH3 phantom and in the skeleton of the UFHADM phantom.

Skeletal region	ICRP-based Cortical bone (cm^3)	MASH3 Cortical bone (cm^3)	UFHADM Cortical bone (cm^3)	ICRP-based Spongiosa (cm^3)	MASH3 Spongiosa (cm^3)	UFHADM Spongiosa (cm^3)	ICRP-based Med. cavity (cm^3)	MASH3 Med. cavity (cm^3)	UFHADM Med. Cavity (cm^3)
Hands	79.7	79.7	92.1	54.7	54.8	49.6			
Radii and Ulnae	86.5	86.5	129.6	93.8	93.8	85.9	59.0	59.0	31.2
Humeri	86.0	86.0	172.6	214.7	214.8	231.2	89.9	89.9	60.5
Ribs	183.9	183.9	124.3	273.0	273.0	186.5			
Sternum	28.8	28.8	19.6	52.2	52.2	45.8			
Scapulae	120.4	120.4	171.1	91.4	91.4	317.8			
Clavicles	22.4	22.4	27.4	29.0	29.0	41.2			
Cervical vertebrae	23.9	32.4	33.8	134.8	124.0	62.8			
Thoracic vertebrae	47.7	64.9	77.4	404.5	386.3	232.1			
Lumbar vertebrae	58.1	58.1	58.5	312.5	312.5	234.1			
Sacrum	65.1	65.1	49.3	182.3	182.3	147.9			
Cranium	422.2	422.2	668.6	249.4	249.4	329.3			
Mandible	42.5	42.5	19.4	26.2	26.2	29.1			
Pelvis	259.9	259.9	231.0	443.1	443.1	693.0			
Femora	197.7	197.7	171.9	667.1	667.2	512.5	277.4	277.4	223.0
Patellae	19.1	19.1	24.7	22.0	22.0	222.0			
Tibiae and fibulae	241.0	241.0	130.5	321.5	321.4	162.6	184.8	184.8	145.6
Feet	221.3	221.3	152.5	143.9	145.1	355.9			
Total volume	2206.0	2231.9	2354.3	3715.9	3688.5	3939.3	611.1	611.1	460.3

Tab 8. Bone site specific volumes for spongiosa, trabecular bone (TB), active marrow (AM), trabecular inactive marrow (TIM), trabecular bone endosteum (TBE), trabecular bone volume fraction (TBVF) and cellularity factor (CF) for the MASH3 and the UFHADM phantoms (Hough et al 2011).

	MASH3							UFHADM						
Trabecular region	Spongiosa (cm^3)	TB (cm^3)	AM (cm^3)	TIM (cm^3)	TBE (cm^3)	TBVF	CF	Spongiosa (cm^3)	TB (cm^3)	AM (cm^3)	TIM (cm^3)	TBE (cm^3)	TBVF	CF
Cranium	249.4	128.4	46.0	75.0	41.3	0.516	0.38	329.3	185.1	54.8	89.4	53.1	0.562	0.38
Mandible	26.2	13.5	4.8	7.9	4.3	0.516	0.38	29.1	2.6	10.1	16.4	2.3	0.089	0.38
Cervical Spine	124.0	13.9	77.1	33.0	11.5	0.113	0.70	62.8	11.2	36.2	15.5	9.2	0.178	0.70
Thoraric Spine	386.4	43.6	239.8	103.0	33.9	0.113	0.70	232.1	21.9	147.1	63.1	21.2	0.094	0.70
Lumbar Spine/Sacrum	494.8	55.6	307.2	132.0	42.9	0.113	0.70	382.0	41.9	238.4	102.2	40.6	0.110	0.70
Pelvis	443.1	93.8	167.7	181.6	61.9	0.212	0.48	693.0	69.3	299.4	324.3	77.3	0.100	0.48
Ribs	273.0	31.2	145.0	96.8	40.9	0.114	0.60	186.5	22.2	115.0	49.3	18.5	0.119	0.70
Sternum	52.2	6.0	27.7	18.5	7.0	0.114	0.60	45.8	3.8	29.4	12.6	4.5	0.083	0.70
Clavicles	29.0	3.3	15.4	10.3	4.1	0.114	0.60	41.2	4.8	21.8	14.6	3.3	0.117	0.33
Scapulae	91.4	10.4	48.5	32.5	13.5	0.114	0.60	317.8	48.6	102.3	166.9	31.8	0.153	0.38
Humeri, proximal	93.4	14.2	19.8	59.4	10.5	0.152	0.25	153.7	14.8	34.7	104.2	12.3	0.096	0.25
Hum,Rad,Uln,Hands	269.9	40.9	0.0	229.0	31.0	0.152		213.0	30.9	0.0	182.0	25.1	0.145	
Femora, proximal	364.8	55.4	77.4	232.0	40.1	0.152	0.25	239.2	35.8	50.9	152.6	29.6	0.150	0.25
Fem,Pat,Fib,Tib,Feet	790.9	120.2	0.0	670.7	88.5	0.152		1013.8	143.4	0.0	870.8	118.2	0.141	
Total	3688.5	630.4	1176.4	1881.7	431.4			3939.3	636.3	1140.1	2163.9	447.0		

Tab 9a. Absorbed fractions in the active marrow of the skeleton from electrons emitted in the active marrow AF(AM←AM) and in the trabecular bone volume AF(AM←TBV) for the MASH3 and the UFHADM phantoms.

Electron	Skeleton									
Energy	MASH3	error	UFHADM	error	Pdif	MASH3	error	UFHADM	error	Pdif
(MeV)	AF(AM←AM)	%	AF(AM←AM)	%	%	AF(AM←TBV)	%	AF(AM←TBV)	%	%
0.01	9.896E-01	0.01	9.85E-01	1.00	0.46	1.321E-03	1.10	1.31E-03	1.00	0.83
0.015	9.774E-01	0.01	9.70E-01	1.00	0.76	2.888E-03	0.73	2.64E-03	1.00	***8.59***
0.02	9.625E-01	0.01	9.51E-01	1.00	1.19	4.725E-03	0.56	4.31E-03	1.00	***8.78***
0.03	9.248E-01	0.01	9.02E-01	1.00	***2.47***	9.527E-03	0.39	8.61E-03	1.00	***9.63***
0.05	8.319E-01	0.02	7.86E-01	1.00	***5.52***	2.225E-02	0.28	1.99E-02	1.00	***10.56***
0.1	6.424E-01	0.03	5.82E-01	1.00	***9.40***	6.031E-02	0.15	5.53E-02	1.00	***8.31***
0.2	5.440E-01	0.03	4.97E-01	1.00	***8.64***	1.348E-01	0.08	1.24E-01	1.00	***8.01***
0.5	4.658E-01	0.02	4.33E-01	1.00	***7.04***	2.065E-01	0.05	1.74E-01	1.00	***15.74***
1	4.227E-01	0.03	3.87E-01	1.00	***8.45***	2.055E-01	0.06	1.67E-01	1.00	***18.73***
1.5	3.900E-01	0.03	3.51E-01	1.00	***10.00***	1.934E-01	0.06	1.55E-01	1.00	***19.86***
2	3.616E-01	0.03	3.19E-01	1.00	***11.78***	1.809E-01	0.06	1.42E-01	1.00	***21.50***
4	2.820E-01	0.04	2.31E-01	1.00	***18.09***	1.412E-01	0.07	1.05E-01	1.00	***25.64***

Tab 9b. Absorbed fractions in the active marrow of the skeleton from electrons emitted in the active marrow AF(AM←AM) and in the trabecular bone volume AF(AM←TBV) for the MASH3* and the UFHADM phantoms.

Electron						Skeleton				
Energy	MASH3*	error	UFHADM	error	Pdif	MASH3*	error	UFHADM	error	Pdif
(MeV)	AF(AM←AM)	%	AF(AM←AM)	%	%	AF(AM←TBV)	%	AF(AM←TBV)	%	%
0.01	9.879E-01	0.01	9.85E-01	1.00	0.29	1.208E-03	1.15	1.31E-03	1.00	-8.44
0.015	9.737E-01	0.01	9.70E-01	1.00	0.38	2.594E-03	0.77	2.64E-03	1.00	-1.77
0.02	9.560E-01	0.01	9.51E-01	1.00	0.52	4.278E-03	0.59	4.31E-03	1.00	-0.75
0.03	9.130E-01	0.01	9.02E-01	1.00	1.20	8.691E-03	0.41	8.61E-03	1.00	0.93
0.05	8.085E-01	0.02	7.86E-01	1.00	***2.78***	2.039E-02	0.29	1.99E-02	1.00	2.40
0.1	6.251E-01	0.03	5.82E-01	1.00	***6.89***	5.746E-02	0.15	5.53E-02	1.00	3.76
0.2	5.414E-01	0.02	4.97E-01	1.00	***8.20***	1.334E-01	0.08	1.24E-01	1.00	***7.05***
0.5	4.646E-01	0.02	4.33E-01	1.00	***6.80***	2.064E-01	0.05	1.74E-01	1.00	***15.70***
1	4.204E-01	0.03	3.87E-01	1.00	***7.94***	2.048E-01	0.06	1.67E-01	1.00	***18.46***
1.5	3.856E-01	0.03	3.51E-01	1.00	***8.97***	1.921E-01	0.06	1.55E-01	1.00	***19.31***
2	3.547E-01	0.03	3.19E-01	1.00	***10.06***	1.785E-01	0.06	1.42E-01	1.00	***20.45***
4	2.620E-01	0.04	2.31E-01	1.00	***11.83***	1.340E-01	0.07	1.05E-01	1.00	***21.64***

Tab 10a. Absorbed fractions in the bone endosteum of the skeleton from electrons emitted in the active marrow AF(BE←AM) and in the trabecular bone volume AF(BE←TBV) for the MASH3 and the UFHADM phantoms.

Electron						Skeleton				
Energy	MASH	error	UFHADM	error	Pdif	MASH	error	UFHADM	error	Pdif
(MeV)	AF(BE←AM)	%	AF(BE←AM)	%	%	AF(BE←TBV)	%	AF(BE←TBV)	%	%
0.01	1.441E-01	0.11	1.21E-01	1.00	***16.03***	2.814E-03	0.75	4.16E-03	1.00	***-47.83***
0.015	1.424E-01	0.11	1.19E-01	1.00	***16.43***	5.994E-03	0.50	8.27E-03	1.00	***-37.97***
0.02	1.408E-01	0.11	1.18E-01	1.00	***16.19***	9.900E-03	0.39	1.34E-02	1.00	***-35.35***
0.03	1.367E-01	0.11	1.14E-01	1.00	***16.61***	1.980E-02	0.27	2.63E-02	1.00	***-32.83***
0.05	1.256E-01	0.12	1.05E-01	1.00	***16.40***	4.439E-02	0.20	5.90E-02	1.00	***-32.91***
0.1	1.029E-01	0.11	8.48E-02	1.00	***17.59***	9.376E-02	0.11	1.25E-01	1.00	***-33.32***
0.2	9.340E-02	0.08	8.11E-02	1.00	***13.17***	1.096E-01	0.07	1.33E-01	1.00	***-21.35***
0.5	8.972E-02	0.05	8.42E-02	1.00	***6.15***	1.025E-01	0.04	1.04E-01	1.00	-1.46
1	8.316E-02	0.04	7.78E-02	1.00	***6.45***	9.357E-02	0.04	9.24E-02	1.00	1.25
1.5	7.691E-02	0.04	7.11E-02	1.00	***7.55***	8.662E-02	0.03	8.42E-02	1.00	***2.79***
2	7.112E-02	0.04	6.52E-02	1.00	***8.32***	8.050E-02	0.03	7.71E-02	1.00	***4.22***
4	5.448E-02	0.04	4.78E-02	1.00	***12.26***	6.156E-02	0.04	5.83E-02	1.00	***5.30***

Tab 10b. Absorbed fractions in the bone endosteum of the skeleton from electrons emitted in the active marrow AF(BE←AM) and in the trabecular bone volume AF(BE←TBV) for the MASH3* and the UFHADM phantoms.

Electron	Skeleton									
Energy	MASH3*	error	UFHADM	error	Pdif	MASH3*	error	UFHADM	error	Pdif
(MeV)	AF(BE←AM)	%	AF(BE←AM)	%	%	AF(BE←TBV)	%	AF(BE←TBV)	%	%
0.01	1.356E-01	0.11	1.21E-01	1.00	***10.77***	2.817E-03	0.75	4.16E-03	1.00	***-47.67***
0.015	1.341E-01	0.11	1.19E-01	1.00	***11.26***	5.997E-03	0.50	8.27E-03	1.00	***-37.90***
0.02	1.331E-01	0.11	1.18E-01	1.00	***11.34***	9.895E-03	0.39	1.34E-02	1.00	***-35.42***
0.03	1.297E-01	0.11	1.14E-01	1.00	***12.10***	1.980E-02	0.27	2.63E-02	1.00	***-32.83***
0.05	1.205E-01	0.12	1.05E-01	1.00	***12.86***	4.442E-02	0.20	5.90E-02	1.00	***-32.82***
0.1	1.013E-01	0.11	8.48E-02	1.00	***16.29***	9.370E-02	0.11	1.25E-01	1.00	***-33.40***
0.2	9.270E-02	0.08	8.11E-02	1.00	***12.51***	1.096E-01	0.07	1.33E-01	1.00	***-21.35***
0.5	8.938E-02	0.05	8.42E-02	1.00	***5.80***	1.024E-01	0.04	1.04E-01	1.00	-1.56
1	8.273E-02	0.04	7.78E-02	1.00	***5.96***	9.336E-02	0.04	9.24E-02	1.00	1.03
1.5	7.623E-02	0.04	7.11E-02	1.00	***6.73***	8.628E-02	0.03	8.42E-02	1.00	***2.41***
2	7.003E-02	0.04	6.52E-02	1.00	***6.90***	7.999E-02	0.03	7.71E-02	1.00	***3.61***
4	5.148E-02	0.04	4.78E-02	1.00	***7.15***	6.014E-02	0.04	5.83E-02	1.00	***3.06***

Tab 11a. AM and BE absorbed dose per air kerma (D/AK) calculated with the192 SPC method and with DRFs for a whole body parallel field of photons incident on the front (AP) of the FASH3 phantom.

	External whole body AP									
FASH3	Active marrow (AM) Skeleton					Bone endosteum (BE) Skeleton				
Photon	192 SPC		DRF		SPC/DRF	192 SPC		DRF		SPC/DRF
Energy	D/AK	Error	D/AK	Error	Pdif	D/AK	Error	D/AK	Error	Pdif
(MeV)	Gy/Gy	%	Gy/Gy	%	%	Gy/Gy	%	Gy/Gy	%	%
0.015	4.906E-04	5.43	5.171E-04	1.97	-5.40	4.055E-04	9.66	4.754E-04	1.66	-17.23
0.02	0.0071	0.78	0.0075	0.66	***-5.63***	0.0084	1.16	0.0103	0.51	***-22.62***
0.03	0.0802	0.42	0.0801	0.28	0.12	0.1221	0.53	0.1499	0.21	***-22.77***
0.04	0.2559	0.41	0.2533	0.21	***1.02***	0.4107	0.51	0.4836	0.15	***-17.75***
0.05	0.4818	0.39	0.4651	0.18	***3.47***	0.7697	0.49	0.8760	0.13	***-13.81***
0.06	0.6679	0.35	0.6423	0.16	***3.83***	1.0630	0.45	1.1717	0.11	***-10.23***
0.07	0.7957	0.32	0.7801	0.15	***1.96***	1.2432	0.42	1.3570	0.11	***-9.15***
0.08	0.8514	0.29	0.8334	0.14	***2.11***	1.2851	0.40	1.3844	0.10	***-7.73***
0.1	0.8997	0.26	0.8821	0.13	***1.96***	1.2677	0.37	1.3345	0.10	***-5.27***
0.15	0.8802	0.32	0.8683	0.13	***1.35***	1.1115	0.46	1.1278	0.09	***-1.47***
0.2	0.8497	0.31	0.8456	0.12	0.48	1.0259	0.44	1.0239	0.09	0.19
0.3	0.8327	0.31	0.8202	0.12	***1.50***	0.9531	0.41	0.9443	0.09	***0.92***
0.5	0.8331	0.31	0.8170	0.12	***1.93***	0.9318	0.35	0.9120	0.09	***2.12***
1	0.8513	0.45	0.8387	0.12	***1.48***	0.9317	0.43	0.9123	0.09	***2.08***
3	0.9349	0.50	0.9008	0.12	***3.65***	0.9878	0.41	0.9503	0.08	***3.80***
6	0.9530	0.52	0.9221	0.12	***3.24***	0.9936	0.41	0.9636	0.08	***3.02***
10	0.9402	0.51	0.9279	0.12	***1.31***	0.9680	0.39	0.9652	0.08	0.29

Tab 11b. AM and BE absorbed dose per air kerma (D/AK) calculated with the 192 SPC method and with DRFs for a whole body parallel field of photons rotational around the vertical body axis (ROT) of the FASH3 phantom.

External whole body ROT

FASH3	Active marrow (AM) Skeleton					Bone endosteum (BE) Skeleton				
Photon	192 SPC		DRF		SPC/DRF	192 SPC		DRF		SPC/DRF
Energy	D/AK	Error	D/AK	Error	Pdif	D/AK	Error	D/AK	Error	Pdif
(MeV)	Gy/Gy	%	Gy/Gy	%	%	Gy/Gy	%	Gy/Gy	%	%
0.015	3.579E-04	5.92	3.162E-04	2.13	11.64	3.779E-04	9.31	3.770E-04	1.64	0.26
0.02	0.0056	0.82	0.0057	0.69	-1.79	0.0071	1.17	0.0086	0.50	***-21.13***
0.03	0.0738	0.40	0.0726	0.30	***1.63***	0.1044	0.53	0.1242	0.21	***-18.97***
0.04	0.2376	0.39	0.2317	0.22	***2.48***	0.3492	0.51	0.4045	0.15	***-15.84***
0.05	0.4364	0.38	0.4230	0.18	***3.07***	0.6564	0.50	0.7371	0.13	***-12.29***
0.06	0.6037	0.34	0.5821	0.17	***3.58***	0.9121	0.45	0.9907	0.12	***-8.62***
0.07	0.7217	0.31	0.7068	0.16	***2.06***	1.0634	0.42	1.1537	0.11	***-8.49***
0.08	0.7730	0.29	0.7545	0.15	***2.39***	1.1069	0.40	1.1748	0.10	***-6.13***
0.1	0.8078	0.26	0.7939	0.14	***1.72***	1.0929	0.37	1.1322	0.10	***-3.60***
0.15	0.7959	0.32	0.7841	0.13	***1.48***	0.9686	0.46	0.9652	0.09	0.35
0.2	0.7760	0.31	0.7680	0.13	***1.03***	0.8900	0.45	0.8803	0.09	***1.09***
0.3	0.7515	0.31	0.7452	0.12	***0.84***	0.8375	0.41	0.8179	0.09	***2.34***
0.5	0.7549	0.30	0.7441	0.12	***1.43***	0.8235	0.35	0.7972	0.09	***3.19***
1	0.7874	0.44	0.7702	0.12	***2.18***	0.8335	0.42	0.8116	0.09	***2.63***
3	0.8687	0.49	0.8381	0.12	***3.52***	0.9080	0.39	0.8657	0.09	***4.66***
6	0.8916	0.51	0.8629	0.12	***3.22***	0.9223	0.39	0.8859	0.09	***3.95***
10	0.8769	0.50	0.8712	0.12	0.65	0.8919	0.38	0.8913	0.09	0.07

Tab 11c. AM and BE absorbed dose per air kerma (D/AK) calculated with the 192 SPC method and with DRFs for an isotropic field of photons incident from the upper hemisphere (ISO2PI) on the FASH3 phantom.

External whole body ISO2PI

FASH3	Active marrow (AM) Skeleton					Bone endosteum (BE) Skeleton				
Photon	192 SPC		DRF		SPC/DRF	192 SPC		DRF		SPC/DRF
Energy	D/AK	Error	D/AK	Error	Pdif	D/AK	Error	D/AK	Error	Pdif
(MeV)	Gy/Gy	%	Gy/Gy	%	%	Gy/Gy	%	Gy/Gy	%	%
0.015	4.339E-04	6.07	4.282E-04	2.10	1.32	5.244E-04	9.04	4.624E-04	1.67	11.82
0.02	0.0056	0.93	0.0058	0.76	-3.57	0.0068	1.35	0.0080	0.56	***-17.65***
0.03	0.0680	0.48	0.0667	0.34	***1.91***	0.0942	0.63	0.1098	0.24	***-16.56***
0.04	0.2139	0.47	0.2082	0.25	***2.66***	0.3152	0.61	0.3605	0.18	***-14.37***
0.05	0.3992	0.45	0.3826	0.21	***4.16***	0.6117	0.58	0.6670	0.15	***-9.04***
0.06	0.5520	0.40	0.5329	0.19	***3.46***	0.8463	0.53	0.9131	0.14	***-7.89***
0.07	0.6597	0.37	0.6449	0.18	***2.24***	1.0002	0.50	1.0651	0.13	***-6.49***
0.08	0.7045	0.34	0.6875	0.17	***2.41***	1.0397	0.47	1.0877	0.12	***-4.62***
0.1	0.7460	0.30	0.7290	0.16	***2.28***	1.0328	0.43	1.0580	0.12	***-2.44***
0.15	0.7290	0.38	0.7258	0.15	0.44	0.9156	0.54	0.9129	0.11	0.29
0.2	0.7142	0.36	0.7139	0.15	0.04	0.8485	0.51	0.8387	0.11	***1.15***
0.3	0.6996	0.36	0.6924	0.15	***1.03***	0.8109	0.47	0.7844	0.11	***3.27***
0.5	0.7158	0.35	0.7060	0.15	***1.37***	0.8096	0.40	0.7870	0.11	***2.79***
1	0.7635	0.50	0.7465	0.15	***2.23***	0.8593	0.47	0.8240	0.10	***4.11***
3	0.8686	0.55	0.8476	0.14	***2.42***	0.9594	0.43	0.9243	0.10	***3.66***
6	0.9225	0.56	0.8871	0.14	***3.84***	1.0077	0.42	0.9648	0.10	***4.26***
10	0.9146	0.56	0.9076	0.14	0.77	0.9878	0.41	0.9832	0.10	0.47

TAB 12. AM and BE absorbed fraction (AF) in the ribs from photons emitted in the lungs of the FASH3 phantom calculated with the 192 SPC method and with DRFs.

Source organ: Lungs										
FASH3	Active marrow (AM) RIBS					Bone endosteum (BE) RIBS				
Photon	192 SPC		DRF		SPC/DRF	192 SPC		DRF		SPC/DRF
Energy	AF	Error	AF	Error	Pdif	AF	Error	AF	Error	Pdif
(MeV)		%		%	%		%		%	%
0.015	1.191E-03	1.28	1.171E-03	0.82	1.68	3.195E-04	2.41	3.392E-04	0.82	***-6.17***
0.02	3.612E-03	0.72	3.584E-03	0.34	0.78	1.018E-03	1.32	1.130E-03	0.34	***-11.00***
0.03	5.228E-03	0.57	5.061E-03	0.18	***3.19***	1.688E-03	0.96	1.873E-03	0.18	***-10.96***
0.05	3.690E-03	0.64	3.520E-03	0.13	***4.61***	1.404E-03	1.01	1.543E-03	0.13	***-9.90***
0.1	2.596E-03	0.51	2.534E-03	0.11	***2.39***	9.472E-04	0.90	9.556E-04	0.11	-0.89
0.2	2.497E-03	0.49	2.477E-03	0.11	0.80	7.642E-04	0.83	7.292E-04	0.11	***4.58***
0.5	2.432E-03	0.51	2.389E-03	0.11	***1.77***	7.175E-04	0.69	6.620E-04	0.11	***7.74***
1	2.227E-03	0.62	2.169E-03	0.11	***2.60***	6.444E-04	0.70	5.966E-04	0.11	***7.42***
1.5	2.032E-03	0.64	1.968E-03	0.11	***3.15***	5.856E-04	0.67	5.406E-04	0.11	***7.68***
2	1.851E-03	0.64	1.811E-03	0.11	***2.16***	5.358E-04	0.66	4.971E-04	0.11	***7.22***
4	1.432E-03	0.62	1.452E-03	0.11	***-1.40***	4.135E-04	0.62	3.983E-04	0.11	***3.68***